Title

Persistently Elevated mTOR Complex 1-S6 Kinase 1 Disrupts DARPP-32–Dependent D1 Dopamine Receptor Signaling and Behaviors

Journal

Biological Psychiatry, 89(11)

ISSN

0006-3223

Authors

Lin, Raozhou
Learman, Lisa N
Na, Chan-Hyun
et al.

Publication Date

2021-06-01

DOI

10.1016/j.biopsych.2020.10.012

Peer reviewed

HHS Public Access

Author manuscript

Biol Psychiatry. Author manuscript; available in PMC 2022 June 01.

Published in final edited form as:

Biol Psychiatry. 2021 June 01; 89(11): 1058–1072. doi:10.1016/j.biopsych.2020.10.012.

Persistently elevated mTORC1-S6 kinase 1 disrupts DARPP-32-dependent D1 dopamine receptor signaling and behaviors

Raozhou Lin[1], **Lisa N. Learman**[1], **Chan-Hyun Na**[2,3], **Santosh Renuse**[4,5], **Kevin T. Chen**[1], **Po Yu Chen**[1], **Gum-Hwa Lee**[1,†], **Bo Xiao**[1], **Susan M. Resnick**[6], **Juan C. Troncoso**[2,7], **Karen K. Szumlinski**[8], **David J. Linden**[1], **Joo-Min Park**[9], **Alena Savonenko**[7], **Akhilesh Pandey**[4,5], **Paul F. Worley**[1,2,*]

[1]Solomon Snyder Department of Neuroscience, Johns Hopkins University, Baltimore, MD 21205, USA.

[2]Department of Neurology, Johns Hopkins University School of Medicine, Baltimore, MD 21205, USA.

[3]Institute for Cell Engineering, Johns Hopkins University School of Medicine, Baltimore, MD 21205, USA.

[4]Department of Laboratory Medicine and Pathology, Mayo Clinic, 200 First ST SW, Rochester, MN 55905, USA.

[5]Center for Individualized Medicine, Mayo Clinic, 200 First ST SW, Rochester, MN 55905, USA.

[6]Laboratory of Behavioral Neuroscience, National Institute on Aging, Baltimore, MD 21224, USA.

[7]Department of Pathology, Johns Hopkins University School of Medicine, Baltimore, MD 21205, USA.

[8]Department of Psychological and Brain Sciences and the Neuroscience Research Institute, University of California, Santa Barbara, CA 93106, USA.

[9]Center for Cognition and Sociality, Institute for Basic Science, Daejeon 34126, Republic of Korea.

Abstract

Background—The serine-threonine kinase mammalian target of rapamycin complex 1 (mTORC1) is essential for normal cell function but is aberrantly activated in brain in both genetic-developmental and sporadic diseases and is associated with a spectrum of neuropsychiatric symptoms. The underlying molecular mechanisms of cognitive and neuropsychiatric symptoms remain controversial.

*Corresponding author. Phone: 410-502-5489 pworley@jhmi.edu.
†Current address: College of Pharmacy, Chosun University, Gwangju, Republic of Korea.

The authors report no biomedical financial interests or potential conflicts of interest.

Methods—The present study examines behaviors in transgenic models that express Rheb, the most proximal known activator of mTORC1, and profiles striatal phosphoproteomics in a model with persistently elevated mTORC1 signaling. Biochemistry, immunohistochemistry, electrophysiology, and behavior approaches are used to examine the impact of persistently elevated mTORC1 on D1 dopamine receptor (D1R) signaling. The effect of persistently elevated mTORC1 was confirmed using D1-Cre to elevate mTORC1 activity in D1R neurons.

Results—We report that persistently elevated mTORC1 signaling blocks canonical D1R signaling that is dependent on dopamine- and cAMP-regulated neuronal phosphoprotein (DARPP-32). The immediate down-stream effector of mTORC1, ribosomal S6 kinase 1 (S6K1), phosphorylates and activates DARPP-32. Persistent elevation of mTORC1-S6K1 occludes dynamic D1R signaling downstream of DARPP-32 and blocks multiple D1R responses including dynamic gene expression, D1R dependent corticostriatal plasticity, and D1R behavioral responses including sociability. Candidate biomarkers of mTORC1-DARPP-32 occlusion are increased in brain of human disease subjects in association with elevated mTORC1-S6K1 supporting a role for this mechanism in cognitive disease.

Conclusions—mTORC1-S6K1 intersection with D1R signaling provides a molecular framework to understand the effects of pathological mTORC1 activation on behavioral symptoms in neuropsychiatric disease.

Keywords

D1 dopamine receptor; mTORC1; S6K1; DARPP-32; immediate early gene; social behavior

Introduction

The serine-threonine kinase mammalian target of rapamycin (mTOR) is a conserved signaling hub that integrates extracellular and environmental inputs to coordinate cell growth and metabolism (1). Aberrant mTOR complex 1 (mTORC1) signaling is implicated in human brain diseases (2, 3). Hyperactive mTORC1 caused by loss-of-function mutations of mTOR upstream suppressor genes, such as *TSC1/2* and *PTEN*, manifests as a high rate of epilepsy, cognitive impairment, and autism spectrum disorders (ASDs) (4, 5). mTORC1 signaling is also reportedly dysregulated in sporadic diseases associated with cognitive and behavioral symptoms including schizophrenia and neurodegenerative diseases (6–8).

Genetic deletion of mTORC1 signaling suppressor genes *Tsc1*, *Tsc2*, or *Pten* in mouse results in behavioral deficits that can be related to human disease, and mTORC1 inhibitor, rapamycin, can ameliorate certain developmental and behavioral deficits in these models (9–11). Studies suggest that elevated mTORC1 causes “exaggerated” protein synthesis that alters the composition of synapses resulting in “hyperconnectivity” and reduced magnitude of mGluR-LTD (12–14). These effects are thought to be causal for behavioral deficits because they can be mitigated by manipulations that counter mTORC1 actions on cap-dependent protein synthesis, or by treatment with a positive allosteric modulator of mGluR5 (13–15). However, the notion that phenotypes are directly linked to mTORC1 activation is challenged by the observation that deletion of *Rptor*, which encodes Raptor, an essential component of mTORC1, fails to restore sociability in *Pten* knockout mice despite restoration

of mTORC1 activity (16). Moreover, the notion that elevated mTORC1 causes behavioral deficits by exaggerated protein translation is challenged by the observation that mice with neuronal overexpression of eIF4E, an effector of mTORC1 translation initiation, do not exhibit social behavior deficits (17). Further, deletion of *Rictor*, an essential component of mTORC2, disrupts mGluR-LTD, while deletion of *Rptor*, essential for mTORC1, does not (18). Finally, knockout of *Rictor* mitigates behavioral deficits in *Pten* knockout mice (16).

To examine how mTORC1 signaling impacts behavior we considered the possibility that genetic deletion of *Tsc1*, *Tsc2* or *Pten* may impact cellular functions in addition to mTORC1 or cause gene-specific adaptations. Accordingly, we examined transgenic models that express Rheb, the most proximal known activator of mTORC1. Rheb is a small GTPase that directly binds mTORC1 and is obligate for mTORC1 activation (19). We compared behaviors in identically designed mouse models that express either wildtype Rheb [Rheb(WT)], which does not result in significant elevation of mTORC1 due to preserved regulatory mechanisms that control its GTP state, or a point mutant of Rheb [Rheb(S16H)] that reduces its GTPase activity and increases activation of mTORC1 (20, 21). This analysis revealed cognitive and behavioral deficits consequent to elevated mTORC1 activity in brain. An unbiased phosphoproteomic analysis of striatum from mice with elevated mTORC1 activity revealed increased D1R signaling with elevated basal DARPP-32(pT34). Further analysis revealed that mTORC1-S6K1 directly phosphorylates DARPP-32(T34) and activates its downstream signaling. However, dynamic D1R signaling downstream of DARPP-32(pT34) was blocked including D1R dependent gene expression, synaptic plasticity, and D1R-induced locomotor activation. Building on the observation that D1R expressing neurons encode and mediate sociability (22), we confirmed that persistently elevated mTORC1 in D1R neurons produces profound sociability deficits. Finally, we examined human postmortem brain from subjects with Alzheimer's disease (AD) or tuberous sclerosis (TS) and found correlations between elevated mTORC1 activity and DARPP-32 signaling, suggesting disruption of DARPP32-dependent D1R signaling may contribute to behavioral symptoms in these diseases.

Methods and Materials

Detailed methods and materials are available in Supplemental Materials.

Rosa-Myc-Rheb(S16H) and Rosa-Myc-Rheb(WT) mice were generated as described previously (21). In this study, Rheb(S16H) refers to *Rosa-Myc-Rheb(S16H)$^{f/f}$;Nestin-Cre* and D1-Rheb(S16H) refers to *Myc-Rheb(S16H)$^{f/f}$;D1-Cre*. Littermate controls (Ctrl) for Rheb(S16H) and D1-Rheb(S16H) are *Rosa-Myc-Rheb(S16H)$^{f/f}$*. *Rosa-Myc-Rheb(WT)$^{f/f}$;Nestin-Cre* is referred to as Rheb(WT) and *Rosa-Myc-Rheb(WT)$^{f/f}$* is referred as Ctrl. Mice at 6 weeks of age were sacrificed and brains were quickly removed. Brains were either mounted and frozen at −80°C until sectioned for immunohistochemistry (IHC), or striatum was dissected for western blotting (WB) or phosphoproteomics. All procedures were approved by the Animal Care and Use Committee of Johns Hopkins University School of Medicine. Data are shown as mean+/− SEM and were analyzed using GraphPad Prism (GraphPad Software, CA) or Statistica 13.3 (TIBCO Software Inc., CA). Statistical methods are detailed in figure legends.

Results

A mouse model with behavioral deficits resulting from persistent elevation of mTORC1 activity

Transgenic mice expressing Myc-Rheb(S16H) in brain exhibit elevation of mTORC1, as revealed by increased phosphorylated 4E-BP1(T37/46), S6K1(T389), and S6(S240/244) in striatal lysate (Figure 1A–D). In Rheb(WT) mice, mTORC1 activity is not robustly elevated (Figure 1C–D). IHC staining confirmed an increase in mTORC1-S6K1 activity in the striatum of Rheb(S16H) mice, as indicated by increased S6(pS240/244). This was evident in both D1R-expressing neurons, identified by co-labeling with substance P (SP-positive), and presumptive D2R-expressing neurons (SP-negative) (Figure S1A–B).

We examined the impact of mTORC1 activation on sociability using a three-chamber social motivation task. Rheb(S16H) and Ctrl littermates preferred investigating the social object, however, Rheb(S16H) mice investigated the social object significantly less than Ctrl littermates (Figure 1E). To ascertain the reduced social investigation results from hyperactive mTORC1, we tested Rheb(WT) in the same task and found that these animals exhibited preference for social object similar to their Ctrl littermates (Figure 1F). The sociability deficit in Rheb(S16H) mice was further confirmed in a 4-trial social recognition task. Rheb(S16H) mice spent less time interacting with juveniles during habituation stage (trial 1–3). During the dishabituation stage (trial 4), Rheb(S16H) mice exhibited reduced interaction to new juveniles (Figure 1G). In the same task, Rheb(WT) and their Ctrl mice showed expected and similar habituation and dishabituation performances (Figure 1H). Although Rheb(S16H) exhibited higher exploratory activity when compared with Rheb(WT), Rheb(S16H) or Rheb(WT) mice exhibited similar levels of novelty induced exploration in open field as their littermate controls, suggesting that the impaired sociability in Rheb(S16H) was not caused by depressed explorative activity (Figure S1C–D). In novel object recognition task, Rheb(S16H) and Ctrl mice spent similar time exploring objects during the learning session when two identical objects were presented (Figure 1I). However, in the testing session where a novel object replaced one of the familiar objects, Rheb(S16H) failed to distinguish between these objects (Figure 1J). These data validate the Rheb(S16H) mouse as a model of sociability and cognitive deficits resulting from persistent elevation of mTORC1 activity.

Persistent elevation of mTORC1 activity causes overrepresentation of D1R signaling

To assess the molecular basis of behavioral deficits linked to mTORC1 activation, we performed an unbiased quantitative phosphoproteomic analysis of Rheb(S16H) and focused on striatum because of its prominent role in social behaviors (22, 23). Among >7,000 phosphopeptides quantified, ~1,600 phosphopeptides were significantly altered (Figure 2A and Table S1). Motif-X analysis (https://motif-x.med.harvard.edu/motif-x.html) of up-regulated phosphosites revealed the most highly enriched motifs corresponded to phosphorylation target sites of mTOR kinase, TP(pT), and S6K1, RxxS(pS) (Figure 2B) (24, 25). We verified enrichment of phosphorylated motifs with antibodies selective for RxxS/T(pS/T), RRxS/T(pS/T) and LxRxxS/T(pS/T) in striatal lysate of Rheb(S16H) (Figure S2A–D).

Among the overrepresented motifs, we noted that the RRxS(pS) epitope is shared with PKA. D1R-activated PKA phosphorylates a panel of substrates, including DARPP-32, to amplify and sustain its effect (26). Putative D1R-targeted phosphopeptides (27) from Rheb(S16H) striatum exhibited enrichment in the group of globally up-regulated sequences (Figure 2C). The cumulative distribution of the fold change of these D1R-targeted phosphopeptides exhibited a significant shift towards up-regulation when compared with overall phosphopeptides at the same level of abundance (Figure 2D). We then extracted the differentially expressed phosphopeptides and input their annotated genes into Ingenuity Pathway Analysis (IPA) and KEGG Pathway Analysis. Both analyses highlighted a set of enriched pathways that are notable for their role in dopamine receptor signaling (Figure 2E, F, and Table S2).

Persistent elevation of mTORC1 increases DARPP-32(pT34) and its nuclear localization

Among the enriched pathways, DARPP-32 signaling was highlighted. D1R-activated PKA phosphorylates DARPP-32 at T34 and indirectly causes dephosphorylation of DARPP-32(T75) via B56/PP2A. In response to psychostimulants, levels of DARPP-32 phosphorylation at T34 and T75 are reciprocally dynamic (28). DARPP-32(pT34) potently inhibits PP1, which increases MAPK signaling to amplify D1R signaling (Figure 3A) (28–31). We observed reductions of two phosphopeptides corresponding to DARPP-32(pT75) in the Rheb(S16H) striatal phosphoproteomic data set (Figure S2E–F) and confirmed this finding together with elevation of DARPP-32(pT34) in Rheb(S16H) striatum by WB (Figure 3B, C). This elevation did not appear to be due to hyperactive PKA because Rheb(S16H) did not alter basal cAMP (Figure 5B) or the PKA substrate GluA1(pS845) (Figure 3B, C). DARPP-32(pT34) was not increased in the striatum of Rheb(WT) (Figure 3B, C).

To evaluate the prediction that elevated mTORC1 increases DARPP-32 activation, we examined DARPP-32(pT34) nuclear entry (32). Biochemical fractionation confirmed that DARPP-32 is present in both cytoplasmic and nuclear fractions (Figure S3D), and further demonstrated that both total and phosphorylated forms DARPP-32 are increased in the soluble nuclear fraction of Rheb(S16H) striatum compared to Ctrl littermates (Figure 3D, E). The nuclear enrichment of DARPP-32(pT34) was further confirmed by IHC, which demonstrated elevated DARPP-32(pT34) in both SP positive and negative neurons (Figure 3F, G). IHC revealed an increase in foci number and intensity of Histone H3(pS10) in the nucleus accumbens (NAc) of Rheb(S16H) mice and was confirmed by WB of Histone H3(pS10) in the chromatin-bound biochemical fraction of Rheb(S16H) striatum (Figure 3H–L).

S6K1 directly phosphorylates DARPP-32

DARPP-32(T34) conforms to the conserved S6K1 phosphorylation consensus motif RxRxxT (Figure 4A) (25). Using an *in vitro* kinase assay, we found that constitutively active S6K1 phosphorylates recombinant GST-DARPP-32(T34), as revealed by WB with antibodies specific to DARPP-32(pT34) and to phospho-motif RxRxxS/T(pS/T). Multiple negative controls included deletion of amino acids 1–80 and point mutant T34A (Figure 4B). Additionally, S6K1 inhibitors PF-4708671 or LY-2584702 completely blocked phosphorylation, as did an inactive analogue of ATP, AMP-PNP (Figure S4A).

To test whether S6K1 can phosphorylate DARPP-32 in cells, we co-transfected DARPP-32 with S6K1 in HEK293FT cells. DARPP-32(pT34) was robustly elevated when co-expressed with constitutively active S6K1(E389ΔCT), compared to co-expression with either wild-type (WT) or inactive mutant S6K1(F5A). The activity of S6K1 wild-type and mutants was confirmed by the phosphorylation of its immediate substrate S6(S240/244). The efficacy of S6K1(WT) to phosphorylate DARPP-32(pT34) was markedly enhanced by co-expression of Rheb(S16H) (Figure 4C, D). Rheb(S16H)-driven hyperphosphorylation of DARPP-32(T34) was reduced by PF-4708671 or LY-2584702, as well as by an AGC kinase inhibitor H89, but not reduced by p90RSK inhibitor, SL0101–1 (Figure S4B, C).

To test whether elevated basal DARPP-32(pT34) in Rheb(S16H) striatum is caused by hyperactive mTORC1-S6K1, we treated Rheb(S16H) mice with PF-4708671. We confirmed a previous report that a single dose of PF-4708671 acutely inhibits S6K1 activity (33), as indicated by a reduction of S6(pS240/244) and concurrent increase of S6K1(pT389) in the striatum of Rheb(S16H) mice. Elevated DARPP-32(pT34) in Rheb(S16H) was reduced by acute PF-4708671 treatment, while GluA1(pS845) was not altered, suggesting that the reduction of DARPP-32(pT34) was caused by PF-4708671 inhibition of S6K1, instead of off-target inhibition of PKA (Figure 4E, F). Taken together, these data indicate that DARPP-32 is a substrate of mTORC1-S6K1 *in vivo*.

mTORC1-S6K1 occludes dynamic DARPP-32 phosphorylation *in vitro and in vivo*.

To model the impact of persistently elevated mTORC1-S6K1 on DARPP-32 phosphorylation, we reconstituted S6K1-DARPP-32 in HEK293FT cells and treated cells with forskolin, which activates adenylyl cyclase (AC) to produce cAMP, or isoproterenol, which activates endogenous Gαs/AC/PKA signaling. Cells transfected with DARPP-32 and S6K1 showed marked increases of DARPP-32(pT34) and PP1α(pT320) upon stimulation with forskolin. By contrast, cells transfected with Rheb(S16H), DARPP-32, and S6K1 showed elevated basal DARPP-32(pT34) and PP1α(pT320), but diminished responses of these phosphosites upon forskolin stimulation (Figure S5A, B). Co-transfection of constitutively active S6K1(E389ΔCT) with DARPP-32 similarly reduced dynamic phosphorylation of DARPP-32(T34) by isoproterenol. The observed effect of elevated mTORC1-S6K1 to mimic Gαs GPCR or AC activation and increase DARPP-32 phosphorylation yet block dynamic increases indicates occlusion of DARPP-32 signaling (Figure S5C, D).

To examine the effect of persistently elevated mTORC1 on DARPP-32 signaling *in vivo*, we treated Rheb(S16H) mice and their Ctrl littermates with amphetamine. Striatum tissues were collected 20 min after treatment to capture the immediate activation of D1R-DARPP-32 signaling (Figure 5A) (28, 29). Amphetamine induced similar levels of dopamine release and cAMP production in Rheb(S16H) striatum when compared with their Ctrl littermates, suggesting that D1R-cAMP signaling axis is not diminished by persistently elevated mTORC1 activity (Figure 5B and Figure S5E). Basal levels of DARPP-32(pT34) and PP1α(pT320) were increased in Rheb(S16H) striatum; however, neither phosphosite changed in response to amphetamine. In the striatum, D1R-DARPP32(pT34) mediated inhibition of PP1 increases pErk, which phosphorylates mGluR5 and contributes to

dopamine's action at the synapse (30, 34). Consistent with occlusion of this pathway in Rheb(S16H) striatum, basal levels of Erk1/2(pT202/Y204) and mGluR5(pS1126) were increased and were not further increased by amphetamine (Figure 5C, D).

Persistent elevation of mTORC1-S6K1 disrupts D1R responses *in vivo*.

We asked if physiological responses to D1R activation would correspond to the elevated basal DARPP-32. We first examined the nucleosome response and found that Histone H3(pS10) was elevated at 60 min after amphetamine treatment in Ctrl mice, but not in Rheb(S16H) mice (Figure 6A, B). Consistent with the notion that the nucleosome response is critical to regulate dynamic gene expression (32), the induction of *Homer1a* and *Npas4* were disrupted in Rheb(S16H) mice (Figure 6C).

We next examined D1R-mediated plasticity of cortico-striatal synapses. We confirmed that HFS induced cortico-striatal LTP, and that subsequent low frequency LFS induced depotentiation in field recordings of acute striatal slices from Ctrl and Rheb(S16H) mice (Figure 6D, E). The LFS induced depotentiation is prevented by prior activation of D1R (35) and is mediated by MAPK dependent phosphorylation of mGluR5 in combination with induction of *Homer1a* (34). In Rheb(S16H) slices SKF38393 failed to block depotentiation, indicating failure of this D1R-mediated synaptic mechanism (Figure 6F, G). Control experiments provided further evidence of specificity of D1R deficits by demonstrating preservation of plasticity of the hippocampus Schaffer-CA1 synapse including mGluR-dependent LTD, low-frequency LTD, theta burst LTP, and high-frequency tetanus LTP in Rheb(S16H) mice (Figure S6A–D).

Lastly, we monitored locomotor activity in Rheb(S16H) mice. Amphetamine induced robust locomotor activation in Ctrl mice but not in Rheb(S16H) mice beginning at 20 min after administration. This time course suggests a physiological role for mTORC1-S6K1-DARPP-32 signaling that is normally manifest later in the response and is disrupted in Rheb(S16H) mice (Figure 6H). Consistent with this premise, rapamycin pretreatment reduced locomotor responses to amphetamine in Ctrl mice but did not alter the response in Rheb(S16H) mice (Figure S6E). To assess mTORC1's impact on D1R signaling, we administered the D1R selective agonist SKF-81297 and found a reduced locomotor response in Rheb(S16H) mice (Figure 6I). Rheb(S16H) and Ctrl mice showed similar locomotor activation in response to the NMDA receptor antagonist MK-801 (0.3 mg/kg, i.p.), indicating a selective impact of persistent elevation of mTORC1 activity on D1R-dependent locomotion (Figure S6F).

Persistent elevation of mTORC1 activity in D1R expressing neurons causes social interaction deficits.

D1R neurons of the mesocorticolimbic circuitry mediate reward processing and integrate neuromodulatory inputs that influence social behaviors (22, 23), and selective disruption of D1R has been linked with social deficits (36–39). We asked if selective increase of mTORC1 in D1R neurons is sufficient to recreate this phenotype. We used D1-Cre to drive Rheb(S16H) expression in D1R-expressing neurons (40) and confirmed the elevation of mTORC1, as shown by increase of S6(pS240/244), and the suppression of mTORC2, as

shown by reduction of Akt(pS473), in the striatum of D1-Rheb(S16H) mice. D1-Rheb(S16H) exhibited robust elevation of basal DARPP-32(pT34) while GluA1(pS845) was not altered (Figure 7A, B).

D1-Rheb(S16H) mice exhibited normal novelty induced locomotor activation in open field as well as in the testing chamber during habituation, but reduced amphetamine induced locomotor activation (Figure 7C and Figure S7A, B). In the social motivation test, D1-Rheb(S16H) mice failed to distinguish between social and non-social objects (Figure 7D, E). In social novelty test, D1-Rheb(S16H) failed to distinguish between familiar and stranger social objects (Figure 7F, G). D1-Rheb(S16H) exhibited normal recognition of novel objects (Figure S7C, D). Accordingly, social interaction deficits in D1-Rheb(S16H) mice are likely not attributable to failure to recognize familiar and stranger mice. These data demonstrate that persistent elevation of mTORC1 in D1R expressing neurons is sufficient to cause social interaction deficits.

Hyperactive mTORC1-S6K1-DARPP-32 signaling in human brain diseases

A primary goal of our analysis is to identify signaling pathways and biomarkers that can be linked to human cognitive disease. In human TS brain samples (Brodmann area, BA, BA46), levels of S6(pS240/244) and DARPP-32(pT34) were significantly elevated and were positively correlated within the TS cohort but not control cohort (Figure 8A–C). In human AD brain, S6(pSer-240/244) was elevated in the middle frontal gyrus (MFG, BA46) and middle temporal gyrus (MTG, BA21). PP1α(pT320) was increased in AD cohort (Figure 8D and Figure S8A, C), and the level of DARPP-32(pT34) correlated with S6(pS240/244) in the AD group but not in age-matched controls (Figure S8B, D). Combining brain samples from MFG and MTG reveals an increase of DARPP-32(pT34) in AD and strong correlation with S6(pS240/244) in AD but not Ctrl brains (Figure 8E, F). Moreover, *Homer1a* mRNA (measured relative to *Homer1c*), which shows reduced induction in Rheb(S16H) mice, was markedly reduced in AD brain (Figure 8G). These findings suggest that disruption of DARPP-32-dependent D1R signaling may represent an underlying mechanism that contributes to cognitive and behavioral deficits.

Discussion

The present study identifies a signaling node that couples mTORC1-S6K1 with canonical dopamine D1 receptor signaling and acts to occlude DARPP-32 signaling in cells with persistently elevated mTORC1 activity and block D1R responses that are dependent on DARPP-32. In support of this model, we demonstrate that DARPP-32 is a direct substrate of S6K1 *in vitro*, in heterologous cells, and *in vivo*. In normal conditions and in response to an acute stimulus such as amphetamine administration, D1R-cAMP-PKA rapidly phosphorylates DARPP-32(T34), which mediates downstream responses in gene expression, corticostriatal plasticity, and behaviors (Figure 8H). But in the condition of persistently elevated mTORC1-S6K1, basal DARPP-32(pT34) is elevated, accompanied by elevated levels of DARPP-32 pathway mediators including PP1α(pT320) and Erk(pT202/Y204) (Figure 3B–I, and Figure 5C, D). Persistently elevated mTORC1 does not interrupt D1R-

cAMP (Figure 5B) but dynamic DARPP-32(pT34) is occluded resulting in disruption of multiple D1R dependent responses (Figure 8H).

The block of D1R responses consequent to persistent mTORC1 activation poses implications for behaviors and appears relevant for understanding the impact of neuropsychiatric and neurodegenerative diseases that result in elevated mTORC1 signaling. D1R signaling is central to social behavior. Optogenetic activation of the VTA projection to NAc or light-evoked D1R signaling in NAc drives social behaviors in rodents (22). Dopamine is also essential for prefrontal cortex function that mediates working memory (41, 42), and cortex-dependent working memory and memory flexibility appear vulnerable to disrupted mTORC1 (43–45). Data in the present study suggests that mTORC1 becomes a driver for DARPP-32 signaling in brain of human subjects with TS and AD. AD often presents with symptoms of mild behavioral impairments that include decreased motivation, emotional dysregulation, and social inappropriateness (46). Our analysis focused on human cortical tissue and it will be important to also examine mesolimbic structures that are more directly related to these behavioral symptoms. In our studies D1R-Cre is expressed in cortical, striatal, and mesolimbic areas which precludes a refined analysis of specific circuits and behaviors, however, the conditional Rheb(S16H) model provides an opportunity for this analysis.

The present model may also be relevant to neuropsychiatric symptoms resulting from stress. Chronic stress impacts sociability and is associated with reduction of excitatory input onto D1R expressing neurons in NAc (36, 37, 47–51). Mice that are susceptible to chronic social defeat stress exhibit elevated BDNF signaling as well as increased downstream MAPK signaling in NAc (50, 51). In addition, BDNF protein level is elevated in depressed human postmortem brain samples (50). Given the important role of neurotrophic factor in mediating mTORC1-S6K1 signaling, it is plausible that stress-induced elevation of BDNF signaling in NAc elevates mTORC1-S6K1 and consequently occludes D1R-DARPP-32 signaling as a basis for stress-induced disruption of social behaviors. Stress also prominently interacts with drug addiction (52) and schizophrenia (53); diseases in which dopamine signaling plays a central role.

Several compelling questions arise from the current study. What is the mechanism for occlusion of D1R-DARPP-32 signaling? D1R-PKA appears intact and elevated DARPP-32(pT34) in Rheb(S16H) mice is reduced by S6K1 inhibition (Figure 3). One possibility is an up-regulation of phosphatase acting at DARPP-32(pT34) in response to elevated mTORC1-S6K1 that secondarily prevents PKA-indued increases. Heterologous cell reconstitution of mTORC1-DARPP-32 interactions may be useful to define this mechanism. A related question is whether mTORC1 signaling contributes to normal D1R responses. The fact that rapamycin reduces amphetamine-induced locomotion in wild-type mice (Figure S6E) suggests this possibility, but further analysis is required. Another question is whether persistently elevated mTORC1 impacts D2R responses and if so, how this might contribute to behavioral phenotypes. Indeed, DARPP-32 is activated by ß-adrenergic and serotonin receptors, as well as hormones acting through non-cAMP-dependent pathways (29, 54), suggesting a broader role for mTORC1-S6K1-DARPP-32 interaction.

Previous studies have offered alternative models for cognitive deficits related to elevated mTORC1 that include changes to cap-dependent protein synthesis and the composition of synapses (12–14). While our findings are not directly contradictory, we did not detect changes in LTP or LTD in the hippocampus or corticostriatal synapses (Figure 6D, E and Figure S6A–D). We note that S6K1 is a component of the protein translation initiation complex (55) and its phosphorylation of DARPP-32 may be sensitive to manipulations used experimentally to implicate translational pathways. mTORC1-S6K1-DARPP-32-PP1 rationalizes increased MAPK (Erk) observed in mouse models with elevated mTORC1 activity including *Tsc* and f*mr1* mice (56, 57). Our findings do not exclude the possible involvement of 4EBP1-eIF4E in the phenotypes of Rheb(S16H) mice, however, it is reported that a mouse model with neuronal overexpression of eIF4E fails to recapitulate social deficits (17). The requirement for dynamic mTORC1-S6K1 coupling with D1R signaling may rationalize the finding that *Rptor* knockout fails to restore social deficits in *Pten* mice since the disruption of mTORC1 does not restore the dynamic coupling, although it reverses mTORC1-S6K1 hyperactivity (16). The complexity of signaling and adaptation highlights the challenge for developing effective therapeutics to mitigate the effect of persistently elevated mTORC1 activity.

Supplementary Material

Refer to Web version on PubMed Central for supplementary material.

Acknowledgments and Disclosures

The authors thank members of the Worley laboratory, especially Drs. W. Zhang, M. Xiao, J. Zhou, L. Yang and Mr. A. Platero for insightful discussion of this project, and Ms J. Zhang and C. Yang for helping with mouse maintenance. This study was supported by funding from NIH (R01 DA010309 and P50DA044123, to P.F.W.). Data are stored and curated on a secure server located in the Worley laboratory in the Department of Neuroscience and Department of Pathology at Johns Hopkins University. Data will be made available upon request.

References

1. Saxton RA, Sabatini DM (2017): mTOR Signaling in Growth, Metabolism, and Disease. Cell. 168:960–976. [PubMed: 28283069]
2. Lipton Jonathan O, Sahin M (2014): The Neurology of mTOR. Neuron. 84:275–291. [PubMed: 25374355]
3. Costa-Mattioli M, Monteggia LM (2013): mTOR complexes in neurodevelopmental and neuropsychiatric disorders. Nat Neurosci. 16:1537. [PubMed: 24165680]
4. Curatolo P, Moavero R, de Vries PJ (2015): Neurological and neuropsychiatric aspects of tuberous sclerosis complex. Lancet Neurol. 14:733–745. [PubMed: 26067126]
5. Butler MG, Dasouki MJ, Zhou X-P, Talebizadeh Z, Brown M, Takahashi TN, et al. (2005): Subset of individuals with autism spectrum disorders and extreme macrocephaly associated with germline PTEN tumour suppressor gene mutations. J Med Genet. 42:318–321. [PubMed: 15805158]
6. An W-L, Cowburn RF, Li L, Braak H, Alafuzoff I, Iqbal K, et al. (2003): Up-Regulation of Phosphorylated/Activated p70 S6 Kinase and Its Relationship to Neurofibrillary Pathology in Alzheimer's Disease. Am J Pathol. 163:591–607. [PubMed: 12875979]
7. Nixon RA (2013): The role of autophagy in neurodegenerative disease. Nat Med. 19:983. [PubMed: 23921753]
8. Howell KR, Law AJ (2019): Neurodevelopmental concepts of schizophrenia in the genome-wide association era: AKT/mTOR signaling as a pathological mediator of genetic and environmental programming during development. Schizophr Res. 217:95–104. [PubMed: 31522868]

9. Tsai PT, Hull C, Chu Y, Greene-Colozzi E, Sadowski AR, Leech JM, et al. (2012): Autistic-like behaviour and cerebellar dysfunction in Purkinje cell Tsc1 mutant mice. Nature. 488:647–651. [PubMed: 22763451]
10. Ehninger D, Han S, Shilyansky C, Zhou Y, Li W, Kwiatkowski DJ, et al. (2008): Reversal of learning deficits in a Tsc2+/− mouse model of tuberous sclerosis. Nat Med. 14:843–848. [PubMed: 18568033]
11. Zhou J, Blundell J, Ogawa S, Kwon C-H, Zhang W, Sinton C, et al. (2009): Pharmacological inhibition of mTORC1 suppresses anatomical, cellular, and behavioral abnormalities in neural-specific Pten knock-out mice. J Neurosci. 29:1773–1783. [PubMed: 19211884]
12. Auerbach BD, Osterweil EK, Bear MF (2011): Mutations causing syndromic autism define an axis of synaptic pathophysiology. Nature. 480:63. [PubMed: 22113615]
13. Gkogkas CG, Khoutorsky A, Ran I, Rampakakis E, Nevarko T, Weatherill DB, et al. (2012): Autism-related deficits via dysregulated eIF4E-dependent translational control. Nature. 493:371. [PubMed: 23172145]
14. Santini E, Huynh TN, MacAskill AF, Carter AG, Pierre P, Ruggero D, et al. (2012): Exaggerated translation causes synaptic and behavioural aberrations associated with autism. Nature. 493:411. [PubMed: 23263185]
15. Michalon A, Sidorov M, Ballard Theresa M, Ozmen L, Spooren W, Wettstein Joseph G, et al. (2012): Chronic Pharmacological mGlu5 Inhibition Corrects Fragile X in Adult Mice. Neuron. 74:49–56. [PubMed: 22500629]
16. Chen C-J, Sgritta M, Mays J, Zhou H, Lucero R, Park J, et al. (2019): Therapeutic inhibition of mTORC2 rescues the behavioral and neurophysiological abnormalities associated with Pten-deficiency. Nat Med. 25:1684–1690. [PubMed: 31636454]
17. Xu Z-X, Kim GH, Tan J-W, Riso AE, Sun Y, Xu EY, et al. (2020): Elevated protein synthesis in microglia causes autism-like synaptic and behavioral aberrations. Nat Commun. 11:1797. [PubMed: 32286273]
18. Zhu PJ, Chen C-J, Mays J, Stoica L, Costa-Mattioli M (2018): mTORC2, but not mTORC1, is required for hippocampal mGluR-LTD and associated behaviors. Nat Neurosci. 21:799–802. [PubMed: 29786082]
19. Yang H, Jiang X, Li B, Yang HJ, Miller M, Yang A, et al. (2017): Mechanisms of mTORC1 activation by RHEB and inhibition by PRAS40. Nature. 552:368–373. [PubMed: 29236692]
20. Yan L, Findlay GM, Jones R, Procter J, Cao Y, Lamb RF (2006): Hyperactivation of mammalian target of rapamycin (mTOR) signaling by a gain-of-function mutant of the Rheb GTPase. The Journal of biological chemistry. 281:19793–19797. [PubMed: 16728407]
21. Zou J, Zhou L, Du X-X, Ji Y, Xu J, Tian J, et al. (2011): Rheb1 Is Required for mTORC1 and Myelination in Postnatal Brain Development. Dev Cell. 20:97–108. [PubMed: 21238928]
22. Gunaydin Lisa A, Grosenick L, Finkelstein Joel C, Kauvar Isaac V, Fenno Lief E, Adhikari A, et al. (2014): Natural Neural Projection Dynamics Underlying Social Behavior. Cell. 157:1535–1551. [PubMed: 24949967]
23. Dölen G, Darvishzadeh A, Huang KW, Malenka RC (2013): Social reward requires coordinated activity of nucleus accumbens oxytocin and serotonin. Nature. 501:179–184. [PubMed: 24025838]
24. Hsu PP, Kang SA, Rameseder J, Zhang Y, Ottina KA, Lim D, et al. (2011): The mTOR-Regulated Phosphoproteome Reveals a Mechanism of mTORC1-Mediated Inhibition of Growth Factor Signaling. Science. 332:1317–1322. [PubMed: 21659604]
25. Pearce LR, Komander D, Alessi DR (2010): The nuts and bolts of AGC protein kinases. Nat Rev Mol Cell Biol. 11:9–22. [PubMed: 20027184]
26. Beaulieu J-M, Gainetdinov RR (2011): The Physiology, Signaling, and Pharmacology of Dopamine Receptors. Pharmacol Rev. 63:182–217. [PubMed: 21303898]
27. Nagai T, Nakamuta S, Kuroda K, Nakauchi S, Nishioka T, Takano T, et al. (2016): Phosphoproteomics of the Dopamine Pathway Enables Discovery of Rap1 Activation as a Reward Signal In Vivo. Neuron. 89:550–565. [PubMed: 26804993]
28. Bateup HS, Svenningsson P, Kuroiwa M, Gong S, Nishi A, Heintz N, et al. (2008): Cell type–specific regulation of DARPP-32 phosphorylation by psychostimulant and antipsychotic drugs. Nat Neurosci. 11:932. [PubMed: 18622401]

29. Svenningsson P, Tzavara ET, Carruthers R, Rachleff I, Wattler S, Nehls M, et al. (2003): Diverse Psychotomimetics Act Through a Common Signaling Pathway. Science. 302:1412–1415. [PubMed: 14631045]
30. Valjent E, Pascoli V, Svenningsson P, Paul S, Enslen H, Corvol J-C, et al. (2005): Regulation of a protein phosphatase cascade allows convergent dopamine and glutamate signals to activate ERK in the striatum. Proc Natl Acad Sci U S A. 102:491–496. [PubMed: 15608059]
31. Ahn J-H, McAvoy T, Rakhilin SV, Nishi A, Greengard P, Nairn AC (2007): Protein kinase A activates protein phosphatase 2A by phosphorylation of the B56δ subunit. Proc Natl Acad Sci U S A. 104:2979–2984. [PubMed: 17301223]
32. Stipanovich A, Valjent E, Matamales M, Nishi A, Ahn J-H, Maroteaux M, et al. (2008): A phosphatase cascade by which rewarding stimuli control nucleosomal response. Nature. 453:879. [PubMed: 18496528]
33. Huynh TN, Santini E, Klann E (2014): Requirement of Mammalian Target of Rapamycin Complex 1 Downstream Effectors in Cued Fear Memory Reconsolidation and Its Persistence. J Neurosci. 34:9034–9039. [PubMed: 24990923]
34. Park Joo M, Hu J-H, Milshteyn A, Zhang P-W, Moore Chester G, Park S, et al. (2013): A Prolyl-Isomerase Mediates Dopamine-Dependent Plasticity and Cocaine Motor Sensitization. Cell. 154:637–650. [PubMed: 23911326]
35. Centonze D, Costa C, Rossi S, Prosperetti C, Pisani A, Usiello A, et al. (2006): Chronic Cocaine Prevents Depotentiation at Corticostriatal Synapses. Biol Psychiatry. 60:436–443. [PubMed: 16476411]
36. Lim BK, Huang KW, Grueter BA, Rothwell PE, Malenka RC (2012): Anhedonia requires MC4R-mediated synaptic adaptations in nucleus accumbens. Nature. 487:183–189. [PubMed: 22785313]
37. Francis TC, Gaynor A, Chandra R, Fox ME, Lobo MK (2019): The Selective RhoA Inhibitor Rhosin Promotes Stress Resiliency Through Enhancing D1-Medium Spiny Neuron Plasticity and Reducing Hyperexcitability. Biol Psychiatry. 85:1001–1010. [PubMed: 30955841]
38. Lee Y, Kim H, Kim JE, Park JY, Choi J, Lee JE, et al. (2018): Excessive D1 Dopamine Receptor Activation in the Dorsal Striatum Promotes Autistic-Like Behaviors. Mol Neurobiol. 55:5658–5671. [PubMed: 29027111]
39. Peça J, Feliciano C, Ting JT, Wang W, Wells MF, Venkatraman TN, et al. (2011): Shank3 mutant mice display autistic-like behaviours and striatal dysfunction. Nature. 472:437. [PubMed: 21423165]
40. Zhang J, Zhang L, Jiao H, Zhang Q, Zhang D, Lou D, et al. (2006): c-Fos Facilitates the Acquisition and Extinction of Cocaine-Induced Persistent Changes. J Neurosci. 26:13287–13296. [PubMed: 17182779]
41. Brozoski T, Brown R, Rosvold H, Goldman P (1979): Cognitive deficit caused by regional depletion of dopamine in prefrontal cortex of rhesus monkey. Science. 205:929–932. [PubMed: 112679]
42. Sawaguchi T, Goldman-Rakic P (1991): D1 dopamine receptors in prefrontal cortex: involvement in working memory. Science. 251:947–950. [PubMed: 1825731]
43. Kosillo P, Doig NM, Ahmed KM, Agopyan-Miu AHCW, Wong CD, Conyers L, et al. (2019): Tsc1-mTORC1 signaling controls striatal dopamine release and cognitive flexibility. Nat Commun. 10:5426. [PubMed: 31780742]
44. Choi CH, Schoenfeld BP, Bell AJ, Hinchey J, Rosenfelt C, Gertner MJ, et al. (2016): Multiple Drug Treatments That Increase cAMP Signaling Restore Long-Term Memory and Aberrant Signaling in Fragile X Syndrome Models. Frontiers in behavioral neuroscience. 10:136. [PubMed: 27445731]
45. Chiang ACA, Fowler SW, Savjani RR, Hilsenbeck SG, Wallace CE, Cirrito JR, et al. (2018): Combination anti-Aβ treatment maximizes cognitive recovery and rebalances mTOR signaling in APP mice. The Journal of experimental medicine. 215:1349–1364. [PubMed: 29626114]
46. Wolinsky D, Drake K, Bostwick J (2018): Diagnosis and Management of Neuropsychiatric Symptoms in Alzheimer's Disease. Curr Psychiatry Rep. 20:117. [PubMed: 30367272]

47. LeGates TA, Kvarta MD, Tooley JR, Francis TC, Lobo MK, Creed MC, et al. (2018): Reward behaviour is regulated by the strength of hippocampus-nucleus accumbens synapses. Nature. 564:258–262. [PubMed: 30478293]

48. Francis TC, Chandra R, Friend DM, Finkel E, Dayrit G, Miranda J, et al. (2015): Nucleus accumbens medium spiny neuron subtypes mediate depression-related outcomes to social defeat stress. Biol Psychiatry. 77:212–222. [PubMed: 25173629]

49. Francis TC, Chandra R, Gaynor A, Konkalmatt P, Metzbower SR, Evans B, et al. (2017): Molecular basis of dendritic atrophy and activity in stress susceptibility. Mol Psychiatry. 22:1512–1519. [PubMed: 28894298]

50. Krishnan V, Han MH, Graham DL, Berton O, Renthal W, Russo SJ, et al. (2007): Molecular adaptations underlying susceptibility and resistance to social defeat in brain reward regions. Cell. 131:391–404. [PubMed: 17956738]

51. Berton O, McClung CA, Dileone RJ, Krishnan V, Renthal W, Russo SJ, et al. (2006): Essential role of BDNF in the mesolimbic dopamine pathway in social defeat stress. Science. 311:864–868. [PubMed: 16469931]

52. Ruisoto P, Contador I (2019): The role of stress in drug addiction. An integrative review. Physiol Behav. 202:62–68. [PubMed: 30711532]

53. Sonnenschein SF, Gomes FV, Grace AA (2020): Dysregulation of Midbrain Dopamine System and the Pathophysiology of Schizophrenia. Frontiers in psychiatry. 11:613. [PubMed: 32719622]

54. Snyder G, Girault J, Chen J, Czernik A, Kebabian J, Nathanson J, et al. (1992): Phosphorylation of DARPP-32 and protein phosphatase inhibitor-1 in rat choroid plexus: regulation by factors other than dopamine. J Neurosci. 12:3071–3083. [PubMed: 1494946]

55. Holz MK, Ballif BA, Gygi SP, Blenis J (2005): mTOR and S6K1 Mediate Assembly of the Translation Preinitiation Complex through Dynamic Protein Interchange and Ordered Phosphorylation Events. Cell. 123:569–580. [PubMed: 16286006]

56. Sawicka K, Pyronneau A, Chao M, Bennett MVL, Zukin RS (2016): Elevated ERK/p90 ribosomal S6 kinase activity underlies audiogenic seizure susceptibility in fragile X mice. Proc Natl Acad Sci U S A. 113:E6290–E6297. [PubMed: 27663742]

57. Chévere-Torres I, Kaphzan H, Bhattacharya A, Kang A, Maki JM, Gambello MJ, et al. (2012): Metabotropic glutamate receptor-dependent long-term depression is impaired due to elevated ERK signaling in the ΔRG mouse model of tuberous sclerosis complex. Neurobiol Dis. 45:1101–1110. [PubMed: 22198573]

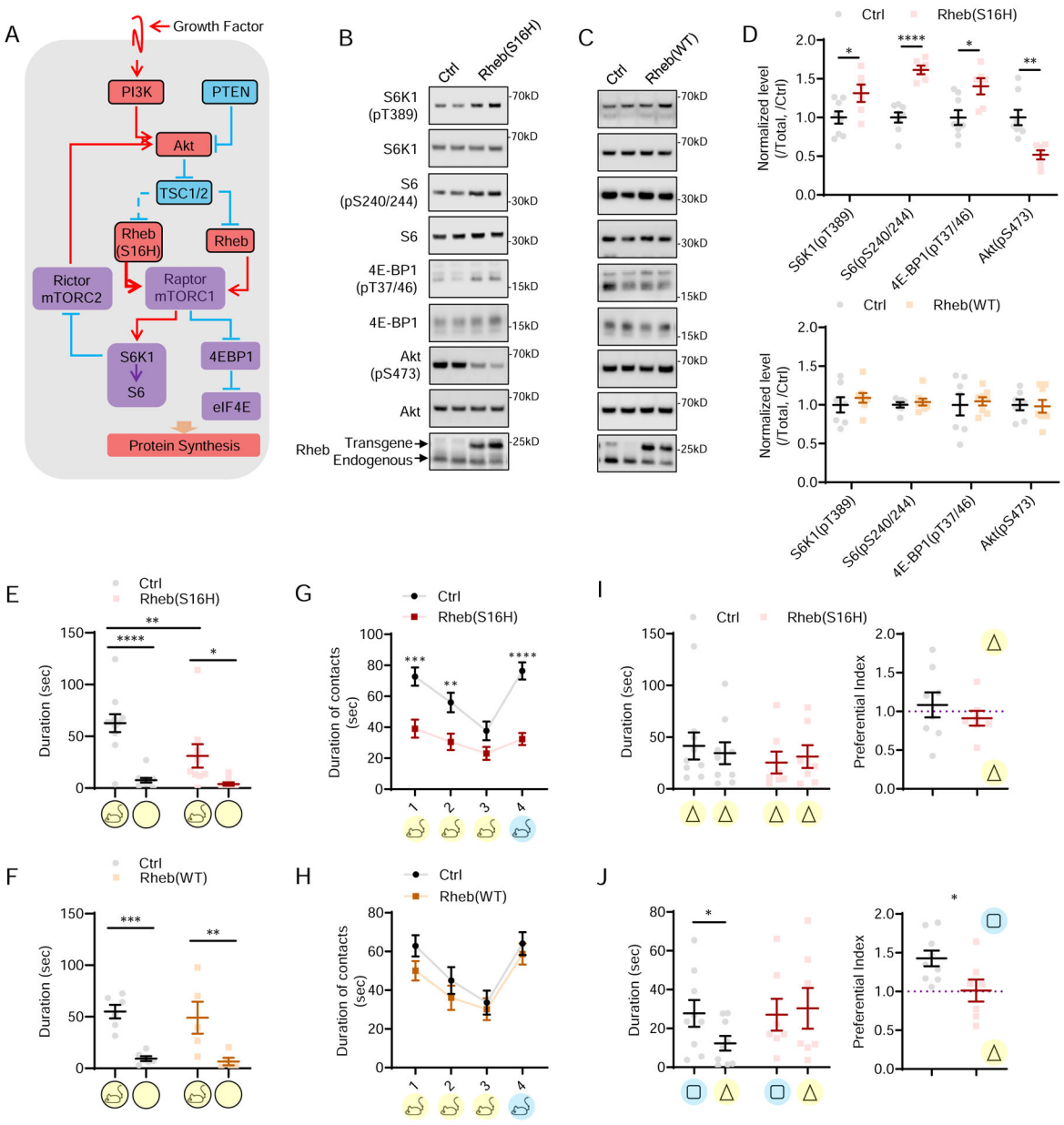

Figure 1. Persistent activation of mTORC1 impairs social and cognitive behavioral domains.

(A) Schematic figure of canonical growth factor signaling activating mTORC1. Rheb acts as a direct and most proximal activator for mTORC1. (B and C) Representative blots and (D) quantification of the WB for the phosphorylation levels of S6K1, S6, 4E-BP1, and Akt in the striatum lysate of (B) Rheb(S16H), (C) Rheb(WT), and their Ctrl littermates, respectively. **P*<0.05, ***P*<0.05 and *****P*<0.0001 by unpaired *t* test; *N*=8 for Ctrl and *N*=6 for Rheb(S16H). *N*=7 for Ctrl and *N*=8 for Rheb(WT). (E) The total time spent investigating social or non-social object by Rheb(S16H) mice and their Ctrl littermates during social motivation task. Statistical significance was determined by two-way mixed-design ANOVA: genotype, **P*=0.0229, objects, *****P*<0.0001; Fisher's *post hoc* test: Ctrl, social vs. empty, *****P*<0.0001; Rheb(S16H), social vs. empty **P*=0.0213; social, Ctrl vs. Rheb(S16H),

**P=0.0035. N=11 for Ctrl, N=9 for Rheb(S16H). (F) The total time spent investigating social or non-social object by Rheb(WT) mice and their Ctrl littermates during social motivation task. Statistical significance was determined by two-way mixed-design ANOVA: objects, **** P<0.0001, genotype, P=0.6622, and interaction, P=0.8124; Fisher's *post hoc* test: Ctrl, social vs. empty, ***P=0.0006; Rheb(S16H), social vs. empty *P=0.0024. N=6 for Ctrl, N=5 for Rheb(WT). (G) The duration of social investigation spent by the Rheb(S16H) mice and the Ctrl littermates during the social recognition task. Two-way mixed-design ANOVA followed by Fisher's *post hoc* test: time, ***P=0.0002; trials, **P=0.0014; Ctrl vs. Rheb(S16H), trial 1, ***P=0.0001, trial 2, **P=0.0023, and trial 4, ****P<0.0001; Ctrl, trial 3 vs. trial 4, ****P<0.0001; Rheb(S16H), trial 3 vs. trial 4, P=0.0814. Data were presented as means ± SEM; N=11 for Ctrl, N=10 for Rheb(S16H). (H) The duration of social investigation by the Rheb(WT) and Ctrl littermates during the social recognition task. Two-way mixed-design ANOVA, trial, ****P<0.0001, genotype, P=0.3092, and interaction, P=0.4736. Data were presented as means ± SEM; N=10 for Ctrl, N=12 for Rheb(WT). (I and J) Novel object recognition task. (left) Time spent on exploring each object and (right) preferential index are shown during the (I) learning session and (J) testing session by Rheb(S16H) mice and the Ctrl littermates. Preferential index is calculated as the ratio for time spent investigating (I) object 1 or (J) novel object to total spent investigating. Statistical significance was determined by two-way ANOVA follow by Bonferroni's *post hoc* test: (J) left, interaction, *P=0.0358; Ctrl, novel vs. familiar, *P=0.0199; right, unpaired t test, *P=0.0208. N=7 for Rheb(S16H) and N=9 for Ctrl littermates. Means ± SEM and/or individual data are presented.

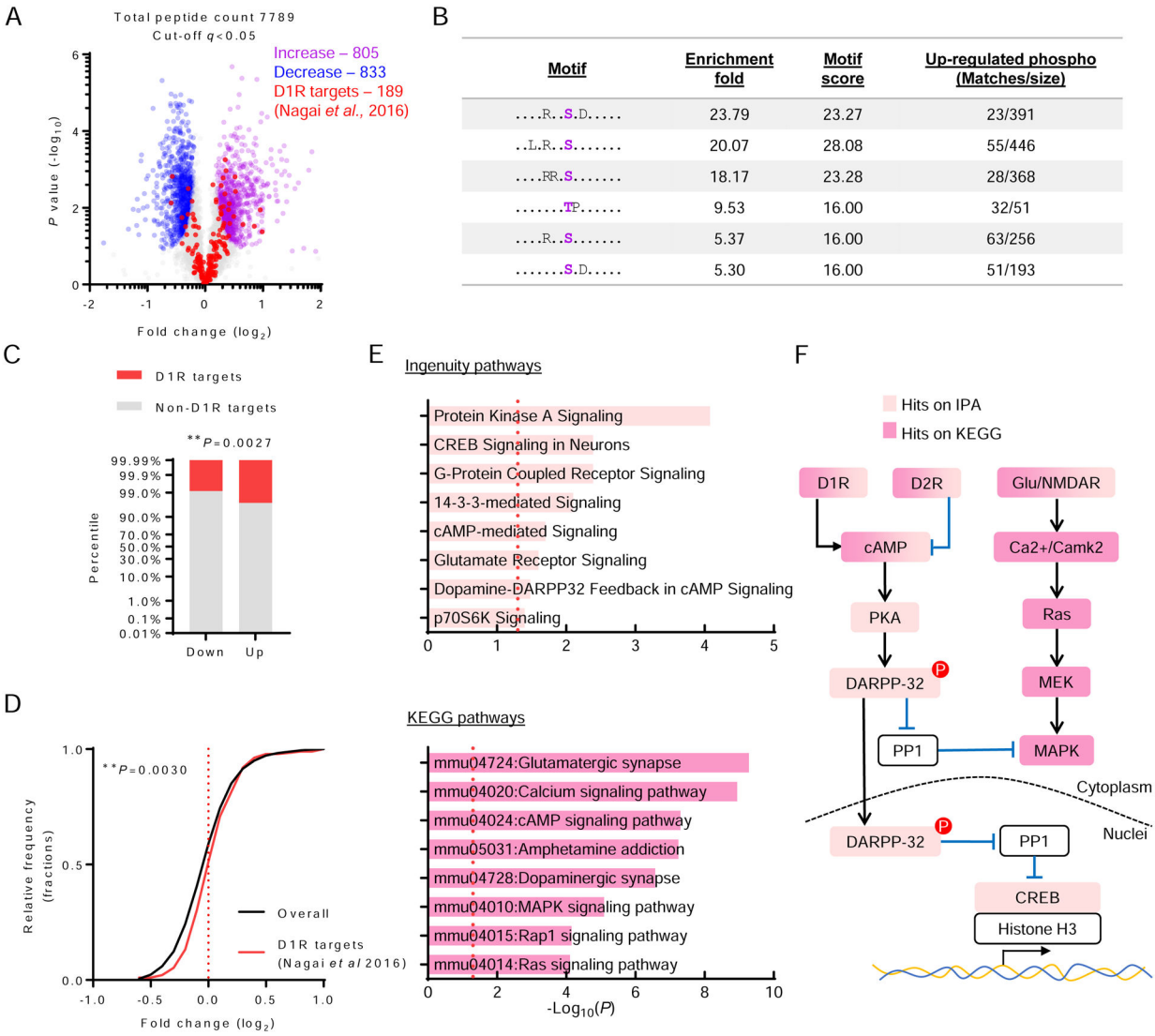

Motif	Enrichment fold	Motif score	Up-regulated phospho (Matches/size)
....R..S.D.....	23.79	23.27	23/391
..L.R..S.....	20.07	28.08	55/446
....RR.S.....	18.17	23.28	28/368
.......TP.....	9.53	16.00	32/51
....R..S.....	5.37	16.00	63/256
.......S.D.....	5.30	16.00	51/193

Figure 2. Phosphoproteomic analysis reveals overrepresentation of D1R-DARPP-32 signaling in Rheb(S16H) striatum.

(A) Volcano plot depicting the relative phosphopeptide abundance in the Rheb(S16H) striatum compared to Ctrl littermates. (B) Motif-X analysis was used to reveal the enriched phosphorylation motifs in the identified phosphopeptides that were significantly (q<0.05) increased in the striatum of Rheb(S16H) mice compared with Ctrl littermates. (C) Comparison of phosphopeptides regulated by D1R activation with robustly altered (q<0.05) expression in Rheb(S16H) striatum versus of Ctrl littermates. 833 phosphopeptides were downregulated in the Rheb(S16H) striatum, 7 of which were D1R targets. 805 phosphopeptides were upregulated in the Rheb(S16H) striatum, 24 of which were D1R targets. There was significantly more D1R targets in the up-regulation group than those in the down-regulation group. ***P*=0.0027 by *Chi* square test with Yate's correction. (D) The cumulative distribution of D1R targets compared to the distribution of total differentially altered phosphopeptides with the same level of abundance in the Rheb(S16H) striatum phosphoproteomic data set. ***P*=0.0030 value was determined by Kolmogorov–Smirnov

test. (E, upper) Shortlisted Ingenuity Pathway Analysis (IPA) and (E, lower) KEGG Pathway Analysis on genes with robustly altered phosphopeptide levels ($q<0.05$). (F) Schematic signaling diagram showing the positive hits in IPA and KEGG analysis in D1/2R- and NMDAR-mediated dopamine signaling.

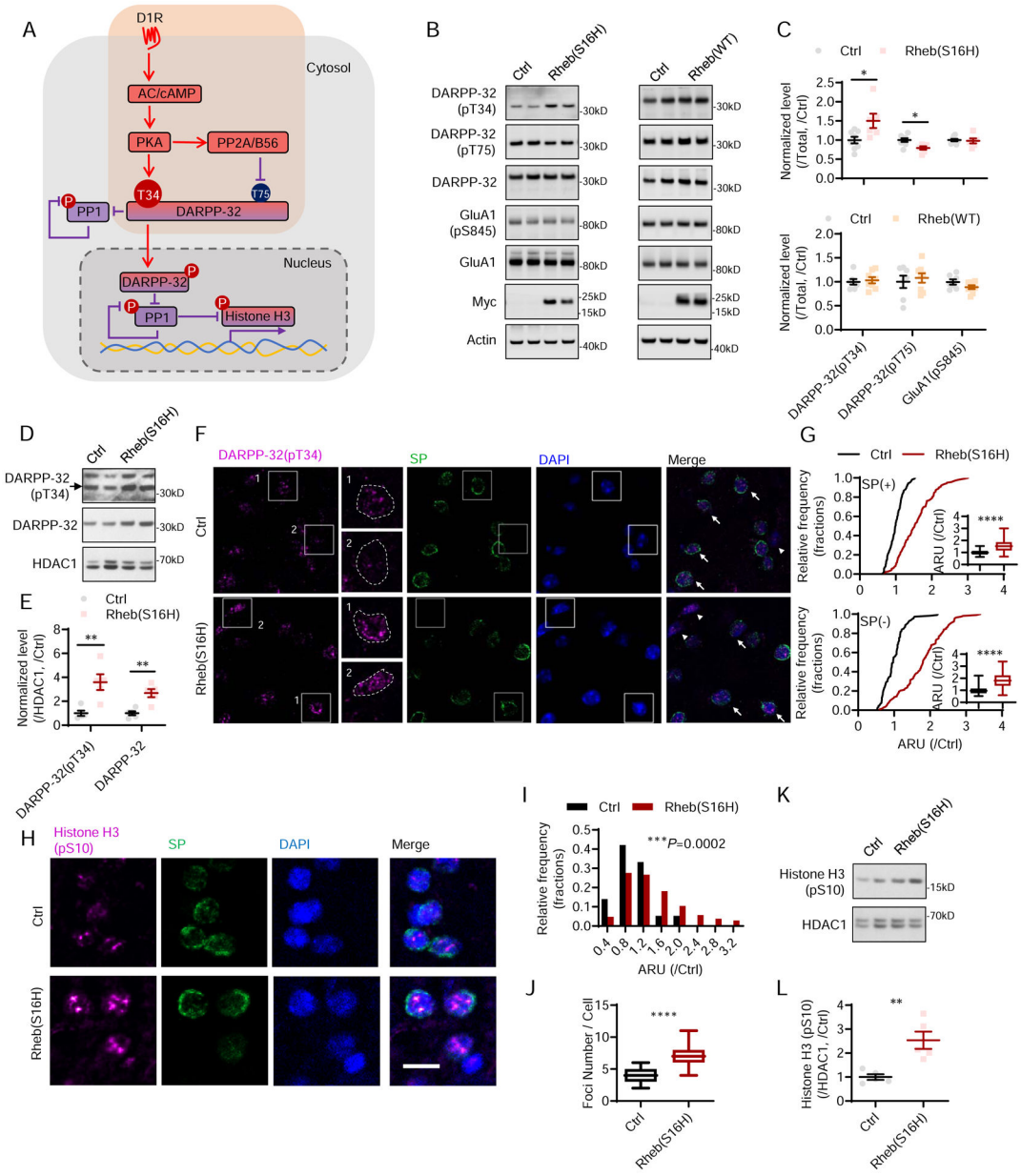

Figure 3. Elevated basal DARPP-32 signaling in Rheb(S16H) striatum.

(A) Schematic figure of canonical D1R-DARPP-32 signaling and its action on nucleosome response. (B) Representative blots and (C) quantification of the phosphorylation levels of DARPP-32(pT34/pT75) and GluA1(pS845) in the striatum lysate of Rheb(S16H) mice or Rheb(WT) mice, and their Ctrl littermates, respectively. *N*=8 for Ctrl and *N*=6 for Rheb(S16H). *N*=7 for Ctrl and *N*=8 for Rheb(WT). **P*<0.05 was determined by unpaired *t* test. (D) Representative blots and (E) quantification of the phosphorylated and total form of DARPP-32 in the nuclear soluble fraction of the striatum of Rheb(S16H) mice and Ctrl littermates. ***P*<0.01 by unpaired *t* test; *N*=5 for each genotype. (F) Representative images and (G) quantification of the immunohistochemistry of DARPP-32(pT34) in NAc of Rheb(S16H) mice and Ctrl littermates. Magenta channel shows DARPP-32(pT34), green

channel shows Substance-P (SP) and blue channel shows DAPI-stained nuclei. SP positive cells are indicated by white arrows and SP negative cells are indicated by white triangles in Merge channel. N=113 cells for Ctrl and N=118 cells for Rheb(S16H); box plot, inter-quartile ± min-max; 3 independent experiments were performed, 4 views were collected per mouse and at least 8 cells were analyzed per view. Scale bar, solid white, 10μm. (H) Representative images and (I and J) quantification of the Histone H3(pS10) foci in the NAc of Rheb(S16H) mice and Ctrl littermates. (I) Relative foci intensity, N=57 for Ctrl and N=105 for Rheb(S16H), ***P=0.0002 by Kolmogorov-Smirnov test; (J) foci number per nuclei, box plot, inter-quartile ± min-max, N=14 neurons for Ctrl, N=15 neurons for Rheb(S16H), ****P<0.0001 by Mann-Whitney U test; data collected from at least 3 mice per genotype. (K) Representative blots and (L) quantification of phosphorylated Histone H3 at Ser-10 in the chromatin-bound fraction of the striatum from Rheb(S16H) mice compared to Ctrl littermates. N=5 for both genotypes.

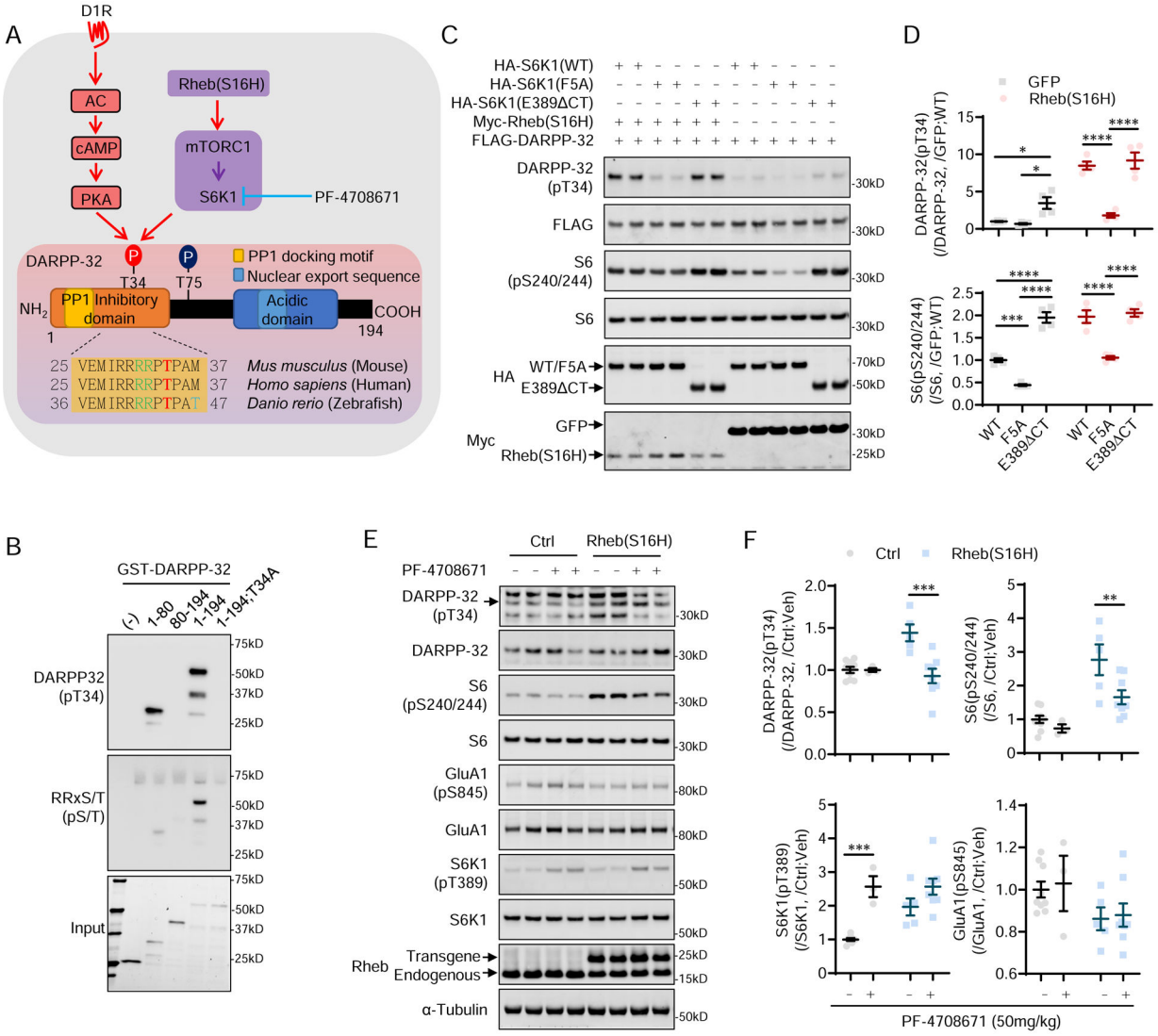

Figure 4. S6K1 directly phosphorylates DARPP-32 and causes elevated basal DARPP-32 signaling in Rheb(S16H) striatum.

(A) Schematic diagram of canonical D1R-DARPP-32 signaling pathway. (B) Representative blots of recombinant GST-tagged wild-type and mutant DARPP-32 incubated with constitutively active S6K1 in a cell-free system. (C) The representative blots and (D) the quantification for the level of DARPP-32 (pT34) and S6 (pS240/244) from the lysate of HEK293FT cells transfected with various combinations of FLAG-DARPP-32, Myc-Rheb(S16H) or Myc-GFP, and wild-type or mutant HA-S6K1 (F5A, inactive; E389ΔCT, constitutively active). Statistical significance was determined by two-way ANOVA followed by Bonferroni's *post hoc* test: DARPP-32(pT34), interaction, ***P=0.0002, GFP/S6K1(WT) vs. GFP/S6K1(F5A), *P=0.0304, GFP/S6K1(F5A) vs. GFP/S6K1(E389ΔCT), *P=0.0135, Rheb(S16H)/S6K1(WT) vs. Rheb(S16H)/S6K1(F5A), ****P<0.0001, Rheb(S16H)/S6K1(E389ΔCT) vs. Rheb(S16H)/S6K1(F5A), ****P<0.0001; S6(pS240/244), interaction, ***P=0.0003, GFP/S6K1(WT) vs. GFP/S6K1(F5A), ***P=0.0007, GFP/S6K1(WT) vs. GFP/S6K1(E389ΔCT), ****P<0.0001, GFP/S6K1(F5A) vs. GFP/S6K1(E389ΔCT),

**** P<0.0001, Rheb(S16H)/S6K1(WT) vs. Rheb(S16H)/S6K1(F5A), **** P<0.0001, Rheb(S16H)/S6K1(E389ΔCT) vs. Rheb(S16H)/S6K1(F5A), **** P<0.0001; N=4 per group. (E) Representative blots and (F) quantification of DARPP-32(pT34), S6(pS240/244), S6K1(pT389), and GluA1(pS845) from the striatal lysate of Rheb(S16H) mice and Ctrl littermates treated with vehicle or PF-4708671. Mice were sacrificed 2 hrs post intraperitoneal injection of PF-4708671 or vehicle, and the striatum was collected and lysed for WB. Statistical significance was determined by two-way ANOVA followed by Bonferroni's *post hoc* test: DARPP-32(pT34), interaction, ** P=0.0046, Rheb(S16H)/vehicle vs. Rheb(S16H)/PF-4708671, *** P=0.0002; S6(pS240/244), treatment, * P=0.0155, Rheb(S16H)/vehicle vs. Rheb(S16H)/PF-4708671, ** P=0.0074; S6K1(pT389), interaction, * P=0.0444, Ctrl/vehicle vs. Ctrl/PF-4708671, *** P=0.0004. N=9 for Ctrl/vehicle, N=3 for Ctrl/PF-4708671, N=5 for Rheb1(S16H)/vehicle, and N=8 for Rheb1(S16H)/PF-4708671. Individual data and means ± SEM are presented.

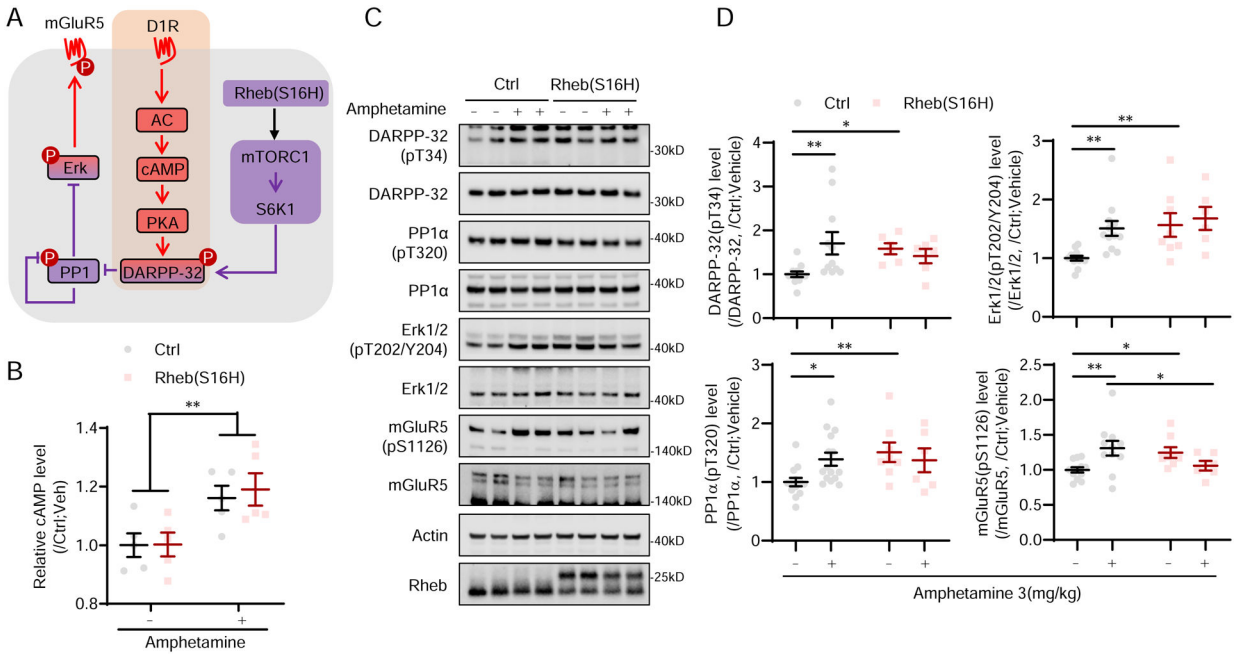

Figure 5. Dynamic DARPP-32 signaling is occluded in Rheb(S16H) striatum.

(A) Schematic of canonical D1R-DARPP-32 signaling dynamic and its action on mGluR5. (B) cAMP production in the striatum of the amphetamine treated Rheb(S16H) mice and Ctrl littermates. Amphetamine (5 mg/kg, i.p.) induced robust cAMP production in both Ctrl and Rheb1(S16H) mice but no difference was found between genotypes (two-way mixed-design ANOVA, treatment, ***P*=0.0013, interaction, *P*=0.2820). *N*=5 for each group. (C) Representative blots and (D) quantification of blots for the phosphorylation levels of DARPP-32, PP1α, Erk1/2, and mGluR5 in the striatum lysate of Ctrl and Rheb(S16H) mice treated with amphetamine (3 mg/kg, i.p.) or vehicle. Striatum was collected 15 min post-injection. Statistical significance was determined by two-way ANOVA followed by Fisher's LSD *post hoc* test: DARPP-32(pT34), interaction, **P*=0.0307, Ctrl/vehicle vs. Rheb(S16H)/vehicle, **P*=0.0389, Ctrl/vehicle vs. Ctrl/amphetamine, ***P*=0.0038; PP1α(pT320), interaction, *P*=0.0561, Ctrl/vehicle vs. Rheb(S16H)/vehicle, ***P*=0.0080, Ctrl/vehicle vs. Ctrl/amphetamine, **P*=0.0151; Erk1/2(pT202/Y204), interaction, *P*=0.1652, Ctrl/vehicle vs. Rheb(S16H)/vehicle, ***P*=0.0048, Ctrl/vehicle vs. Ctrl/amphetamine, ***P*=0.0047; mGluR5(pS1126), interaction, ***P*=0.0047, Ctrl/vehicle vs. Rheb(S16H)/vehicle, **P*=0.0309, Ctrl/vehicle vs. Ctrl/amphetamine, ***P*=0.0040, Ctrl/amphetamine vs. Rheb(S16H)/amphetamine, **P*=0.0485; at least *N*=6 mice per group. Individual data and/or means ± SEM are presented.

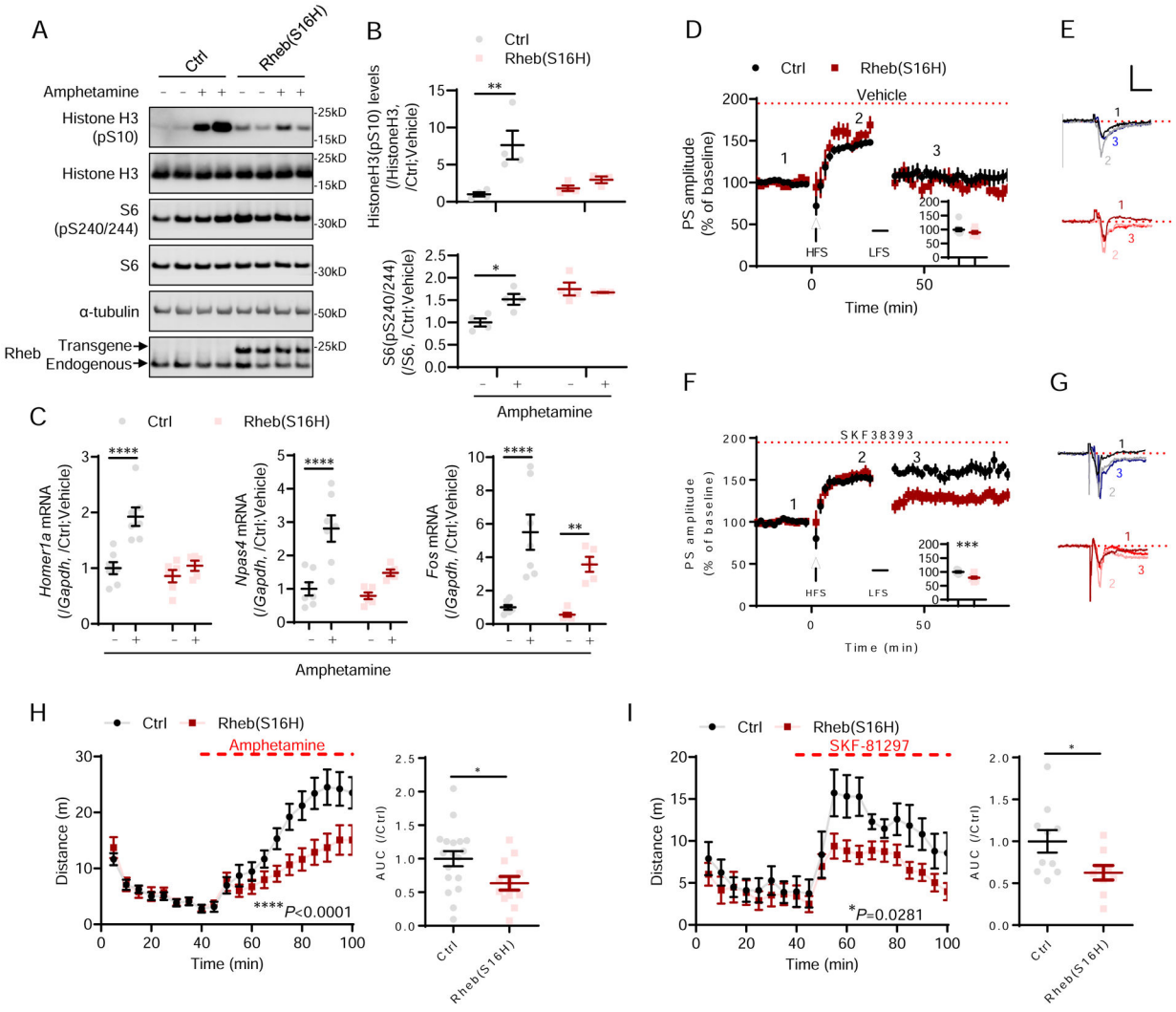

Figure 6. Persistently elevated mTORC1 activity disrupts amphetamine-induced gene expression, and D1R-mediated corticostriatal plasticity and locomotor activation.

(A) Representative blots and (B) quantification of blots for the phosphorylation levels of Histone H3 in the striatum lysate of Rheb(S16H) mice and their Ctrl littermates that were treated with amphetamine (5 mg/kg, i.p.) or vehicle (Saline, i.p.). Striatum was collected 60 min post-injection. Statistical significance was determined by two-way ANOVA followed by Bonferroni's *post hoc* test: Histone H3(pS10), interaction, **P*=0.0289, Ctrl/vehicle vs. Ctrl/amphetamine, ***P*=0.0019; S6(pS240/244), interaction, **P*=0.0237, genotype, ***P*=0.022, Ctrl/vehicle vs. Ctrl/amphetamine, **P*=0.0127. At least *N*=3 per group. (C) The mRNA levels of *Homer1a*, *Npas4* and *Fos* in Ctrl or Rheb(S16H) striatum with amphetamine (5 mg/kg, 60 min, i.p.) treatment. The levels of genes were normalized to the level of *Gapdh* and to the Ctrl/vehicle group. Statistical significance was determined by two-way ANOVA followed by Bonferroni's *post hoc* test: *Homer1a*, interaction, **P*=0.0104, Ctrl/vehicle vs. Ctrl/amphetamine, *****P*<0.0001; *Npas4*, interaction, **P*=0.042, Ctrl/vehicle vs. Ctrl/amphetamine, *****P*<0.0001; *Fos*, interaction, *P*=0.2531, treatment, *****P*<0.0001; at least *N*=3 per group. (D to G) Corticostriatal LTP and depotentiation in field-potential recordings

of brain slices prepared from Rheb(S16H) mice and Ctrl littermates in the presence of (D and E) vehicle or (F and G) the specific D1-like receptor agonist, SKF38393 (3 μM; left). Sample traces (E and G) and the magnitude (E and F, islets) of LFS induced depotentiation of LTP (63–69 min) in the presence of (D and E) vehicle or (F and G) SKF38393. (F) islet, *** P=0.0003 was determined by unpaired t test; Ctrl/vehicle, N=9 slices from 5 mice; Ctrl/SKF38393, N=8 slices from 4 mice; Rheb(S16H)/vehicle, N=6 slices from 4 mice; Rheb(S16H)/SKF38393, N=11 slices from 6 mice; scale bar, 1 mV, 10 ms. (H) Amphetamine (2 mg/kg, i.p.) and (I) SKF-81297 (2.5 mg/kg, i.p.) induced locomotor activity and accumulative distance traveled by Rheb(S16H) mice or Ctrl littermates. Locomotor activation was analyzed in (left) 5-min bins and (right) the total distance traveled after treatment. Two-way mixed-designed ANOVA: left, (H) Amphetamine, interaction, **** P<0.0001, (I) SKF-81297, interaction, * P=0.0281; right, genotype, (H) Amphetamine, * P=0.0306, (i) SKF-81297, * P=0.0354; at least N=9 per group. Individual data and/or means ± SEM are presented.

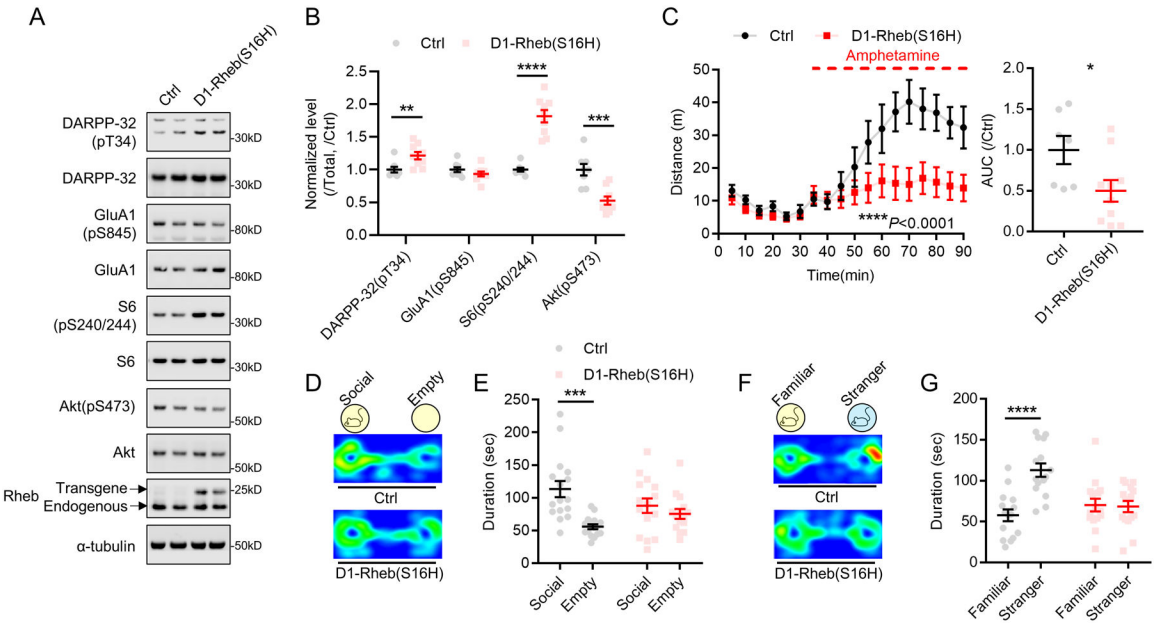

Figure 7. Persistently elevated mTORC1 in D1R neurons evokes social interaction deficit.

(A) Representative blots and (B) quantification of the levels of phosphorylated DARPP-32, GluA1, S6, and Akt, in the striatal lysate of the D1-Rheb(S16H) mice and their Ctrl littermates. ***P*<0.01, ****P*<0.001, and *****P*<0.0001 by unpaired *t* test; *N*=9 for D1-Rheb(S16H) and *N*=8 for Ctrl. (C) Amphetamine (2 mg/kg, i.p.) induced locomotor activation in D1-Rheb(S16H) mice and Ctrl littermates. Two-way mixed designed ANOVA: left, genotype, **P*=0.0377; interaction, *****P*<0.0001; right, unpaired *t* test, **P*=0.0331. At least *N*=7 per group. (D to G) Three-chamber sociability task. (D) Heat map of duration spent on the testing chamber of D1-Rheb(S16H) mice and the Ctrl littermates on social motivation task. (E) Duration of mice spent on investigating social object and empty cup in three-chamber sociability task on D1-Rheb(S16H) mice. Statistical significance was determined by two-way ANOVA followed by Bonferroni's *post hoc* test: interaction, **P*=0.0245; Ctrl, social vs. empty, ****P*=0.0003; D1-Rheb(S16H), social vs. empty, *P*=0.7492. (F) Heat map of duration spent on the testing chamber of D1-Rheb(S16H) mice and the Ctrl littermates on social novelty test. (G) Duration of D1-Rheb(S16H) mice and the Ctrl littermates spent on investigating familiar and stranger social objects. Statistical significance was determined by two-way ANOVA followed by Bonferroni's *post hoc* test: interaction, ****P*=0.0001; Ctrl, stranger vs. familiar, *****P*<0.0001; D1-Rheb(S16H), stranger vs. familiar, *P*>0.9999. *N*=15 for both D1-Rheb(S16H) and Ctrl littermates. Individual data and means ± SEM are presented.

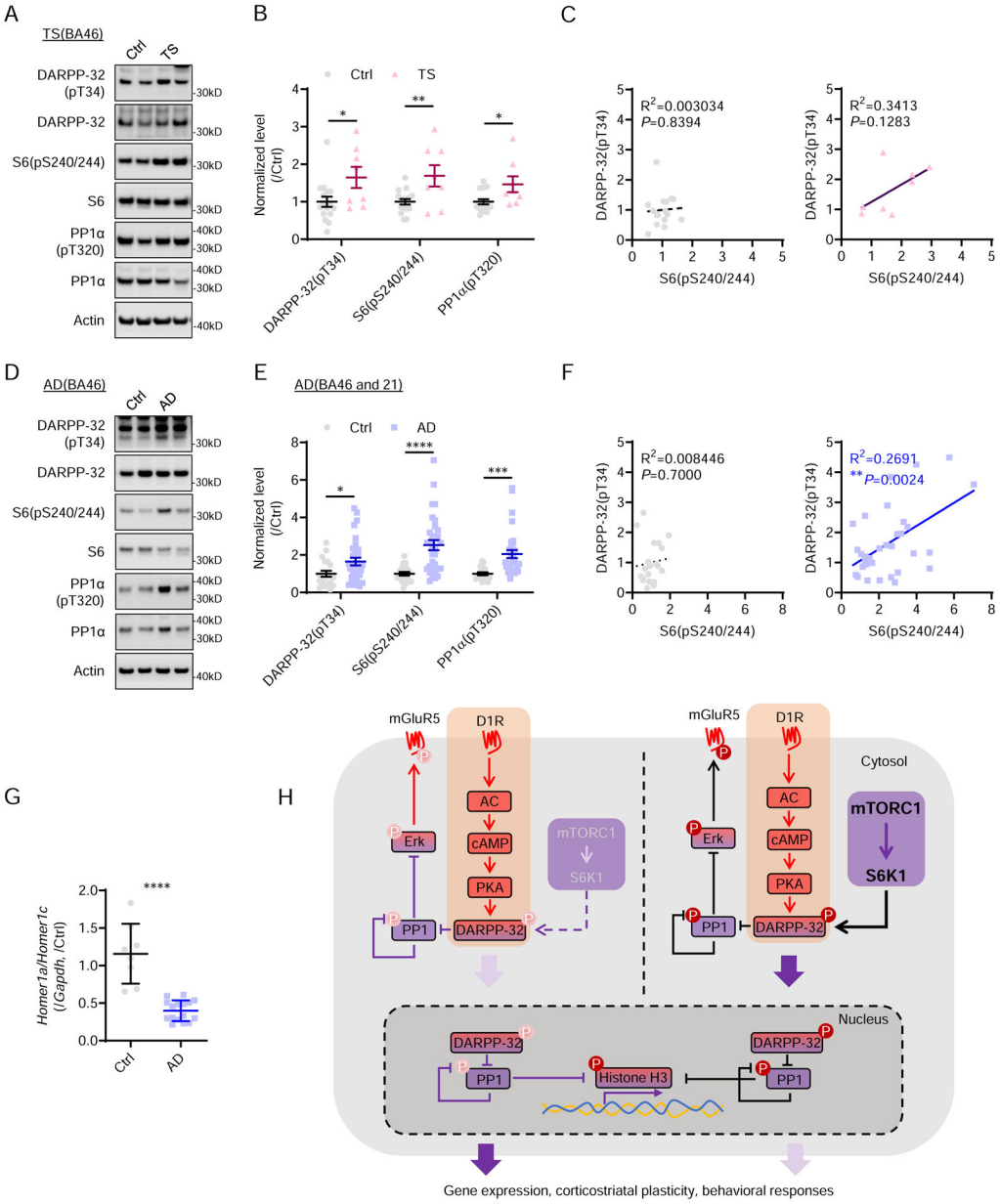

Figure 8. Hyperactive mTORC1-S6K1-DARPP-32 signaling in human brain diseases.

(A) The representative blots and (B) quantification of DARPP-32(pT34), PP1α(pT320), and S6(pS240/244) of the human brain lysate from Brodmann area (BA) 46 of individuals with tuberous sclerosis (TS) and age-matched controls (Ctrl). **P*<0.05 and ***P*<0.01 were determined by unpaired *t* test. (C) The correlation between DARPP-32(pT34) and S6(pS240/244) in Ctrl and TS groups, respectively. *N*=16 for Ctrl, *N*=8 for TS. (D) The representative blots of DARPP-32(pT34), PP1α(pT320), and S6(pS240/244) of the human brain lysate from BA46 of individuals with Alzheimer's disease (AD) and age-matched controls (Ctrl). (E) Quantification of DARPP-32(pT34), PP1α(pT320), and S6(pS240/244) of human brain lysate of AD patients and Ctrl (combining BA46 and BA21). **P*<0.05, ****P*<0.001, and *****P*<0.0001 were determined by unpaired *t* test. (F) The correlation

between DARPP-32(pT34) and S6(pS240/244) in AD patients and Ctrl (combining BA46 and BA21), respectively. *N*=20 for Ctrl, *N*=32 for AD. (G) Ratio of Homer1a relative to Homer1c in human AD brain samples. *N*=8 for Ctrl, *N*=16 for AD. **** *P*<0.0001 were determined by unpaired *t* test. Individual data and/or means ± SEM were presented. (H) Schematic model of mTORC1-S6K1 negatively impacting D1R signaling under condition of persistent elevated mTORC1 activity.

KEY RESOURCES TABLE

Resource Type	Specific Reagent or Resource	Source or Reference	Identifiers	Additional Information
Add additional rows as needed for each resource type	Include species and sex when applicable.	Include name of manufacturer, company, repository, individual, or research lab. Include PMID or DOI for references; use “this paper” if new.	Include catalog numbers, stock numbers, database IDs or accession numbers, and/or RRIDs. RRIDs are highly encouraged; search for RRIDs at https://scicrunch.org/resources.	Include any additional information or notes if necessary.
Antibody	Rabbit polyclonal antibody to DARPP-32(pT34)	PhosphoSolutions	Cat# p1025–34, RRID:AB_2492068	
Antibody	Rabbit polyclonal antibody to DARPP-32(pT75)	Cell Signaling Technology	Cat# 2301, RRID:AB_2169010	
Antibody	Mouse monoclonal antibody to DARPP-32	Santa Cruz Biotechnology	Cat# sc-398144	
Antibody	Rabbit polyclonal antibody to GluA1(pS845)	Novus	Cat# NB 300–171, RRID:AB_350489	
Antibody	Mouse monoclonal antibody to GluA1	Millipore	Cat# MAB2263, RRID:AB_11212678	
Antibody	Mouse monoclonal antibody to Rheb	Santa Cruz Biotechnology	Cat# sc-271509, RRID:AB_10659102	
Antibody	Mouse monoclonal antibody to Actin	Abcam	Cat# ab8226, RRID:AB_306371	
Antibody	Rabbit polyclonal antibody to DARPP-32(pT34)	Novus	Cat# NB 300–224, RRID:AB_350538	
Antibody	Guinea pig polyclonal antibody to Substance P	Abcam	Cat# ab10353, RRID:AB_297089	
Antibody	Rabbit monoclonal antibody to S6K1(pT389)	Cell Signaling Technology	Cat# 9234, RRID:AB_2269803	
Antibody	Mouse monoclonal antibody to S6K1	Santa Cruz Biotechnology	Cat# sc-8418, RRID:AB_628094	
Antibody	Rabbit monoclonal antibody to S6(pS240/244)	Cell Signaling Technology	Cat# 5364, RRID:AB_10694233	
Antibody	Mouse monoclonal antibody to S6	Santa Cruz Biotechnology	Cat# sc-74459, RRID:AB_1129205	
Antibody	Rabbit polyclonal antibody to eIF4G(pS1108)	Cell Signaling Technology	Cat# 2441, RRID:AB_2277632	
Antibody	Rabbit monoclonal antibody to eIF4G	Cell Signaling Technology	Cat# 2469, RRID:AB_2096028	
Antibody	Rabbit monoclonal antibody to Akt(pS473)	Cell Signaling Technology	Cat# 3787, RRID:AB_331170	
Antibody	Mouse monoclonal antibody to Akt	Santa Cruz Biotechnology	Cat# sc-135829, RRID:AB_2224733	
Antibody	Mouse monoclonal antibody to eIF4B	Santa Cruz Biotechnology	Cat# sc-376062, RRID:AB_10988946	
Antibody	Rabbit monoclonal antibody to Histone H3	Cell Signaling Technology	Cat# 4499, RRID:AB_10544537	
Antibody	Rabbit polyclonal antibody to Histone H3(pS10)	Abcam	Cat# ab5176, RRID:AB_304763	
Antibody	Mouse monoclonal antibody to FLAG	Sigma-Aldrich	Cat# P2983, RRID:AB_439685	
Antibody	Rabbit polyclonal antibody to HA	Thermo Fisher Scientific	Cat# 710236, RRID:AB_2532641	
Antibody	Mouse monoclonal antibody to Myc	Thermo Fisher Scientific	Cat# 13–2500, RRID:AB_2533008	
Antibody	Rabbit monoclonal antibody to RRxS/T(pS/T)	Cell Signaling Technology	Cat# 9624, RRID:AB_331817	

Resource Type	Specific Reagent or Resource	Source or Reference	Identifiers	Additional Information
Antibody	Rabbit monoclonal antibody to Raptor	Cell Signaling Technology	Cat# 2280, RRID:AB_561245	
Antibody	hFAB™ Rhodamine Anti-Tubulin Primary Antibody	Bio-Rad	Cat# 12004166	
Antibody	Rabbit monoclonal antibody to GSK3α/β(pS21/9)	Cell Signaling Technology	Cat# 8566	
Antibody	Mouse monoclonal antibody to GSK3α/β	Santa Cruz Biotechnology	Cat# sc-7291, RRID:AB_2279451	
Antibody	Rabbit polyclonal antibody to PP1α(pT320)	Cell Signaling Technology	Cat# 2581, RRID:AB_330823	
Antibody	Mouse monoclonal antibody to PP1α	Santa Cruz Biotechnology	Cat# sc-271762, RRID:AB_10708123	
Antibody	Rabbit monoclonal antibody to PP1α(pT320)	Abcam	Cat# ab62334, RRID:AB_956236	
Bacterial or Viral Strain	NEB 5-alpha Competent E. coli	NEB	Cat# C2988	
Bacterial or Viral Strain	BL21-Gold (DE3) Competent E. coli	Agilent Technologies	Cat# 230132	
Biological Sample	Healthy adult BA46 brain tissue	NIH NeuroBioBank	Request #1323	
Biological Sample	Tuberous sclerosis adult patient BA46 brain tissue	NIH NeuroBioBank	Request #1323	
Biological Sample	Healthy adult BA46/BA9 brain tissue	JHUSOM Brain Resource Center	N/A	
Biological Sample	Alzheimer's patient BA46/BA21 brain tissue	JHUSOM Brain Resource Center	N/A	
Chemical Compound or Drug	D-Amphetamine hemisulfate salt	Sigma-Aldrich	Cat# A5880, CAS 51-63-8	
Chemical Compound or Drug	Rapamycin	LC Laboratories	Cat# R-5000, CAS 53123-88-9	
Chemical Compound or Drug	PF-4708671	Selleckchem	Cat# S2163, CAS 1255517-76-0	
Chemical Compound or Drug	AMP-PNP	Sigma-Aldrich	Cat# A2647, CAS 25612-73-1 (free acid)	
Chemical Compound or Drug	LY-2584702	Selleckchem	Cat# S7704, CAS 1082949-68-5	
Chemical Compound or Drug	SL0101–1	Tocris	Cat# 2250, CAS 77307-50-7	
Chemical Compound or Drug	H 89 dihydrochloride	Tocris	Cat# 2910, CAS 130964-39-5	
Chemical Compound or Drug	Forskolin	Tocris	Cat# 1099, CAS 66575-29-9	
Chemical Compound or Drug	Isoproterenol hydrochloride	Tocris	Cat# 1747, CAS 51-30-9	
Commercial Assay Or Kit	Subcellular Protein Fractionation Kit for Tissues	Thermo Fisher Scientific	Cat# 87790	
Cell Line	HEK293FT	Thermo Fisher Scientific	Cat# R70007	

Resource Type	Specific Reagent or Resource	Source or Reference	Identifiers	Additional Information
Organism/Strain	Mouse: ROSA-Rheb(S16H)	(Zou et al., 2011)		
Organism/Strain	Mouse: ROSA-Rheb(WT)	(Zou et al., 2011)		
Organism/Strain	Mouse: B6.Cg-Rptortm1.1Dmsa/J	Jackson Laboratory	Stock# 013188	
Organism/Strain	Mouse: B6.Cg-Tg(Nes-cre)1Kln/J	Jackson Laboratory	Stock# 003771	
Organism/Strain	Mouse: B6;129-Tg(Drd1-cre)120Mxu/Mmjax	Jackson Laboratory	Stock# 37156-JAX	
Sequence-Based Reagent	Homer1a-Fw, 5'-GAGCCTGTTAGCATTGATGG-3'	This study		
Sequence-Based Reagent	Homer1a-Rv, 5'-CACGGTACGGCCAATAACTA-3'	This study		
Sequence-Based Reagent	Npas4-Fw, 5'-CTGCATCTACACTCGCAAGG-3'	(Madabhushi et al., 2015)		
Sequence-Based Reagent	Npas4-Rv, 5'-GCCACAATGTCTTCAAGCTCT-3'	(Madabhushi et al., 2015)		
Sequence-Based Reagent	Fos-Fw, 5'-GAACGGAATAAGATGGCTGC-3'	(Madabhushi et al., 2015)		
Sequence-Based Reagent	Fos-Rv, 5'-TTGATCTGTCTCCGCTTGG-3'	(Madabhushi et al., 2015)		
Sequence-Based Reagent	Gapdh-Fw, 5'-CTGGAGAAACCTGCCAAGTA-3'	(Hu et al., 2010)		
Sequence-Based Reagent	Gapdh-Rv, 5'-AGTGGGAGTTGCTGTTGAAG-3'	(Hu et al., 2010)		
Recombinant DNA	pRK5-Myc-Rheb(S16H)	(Zou et al., 2011)		
Recombinant DNA	pcDNA3-FLAG-DARPP-32	This study		
Recombinant DNA	pRK7-HA-S6K1-WT	Gift from John Blenis	Addgene plasmid # 8984; RRID:Addgene_8984	
Recombinant DNA	pRK7-HA-S6K1-F5A	Gift from John Blenis	Addgene plasmid # 8986; RRID:Addgene_8986	
Recombinant DNA	pRK7-HA-S6K1-E389-deltaCT	Gift from John Blenis	Addgene plasmid # 8993; RRID:Addgene_8993	
Recombinant DNA	pRK5-Myc-GFP	This study		
Software; Algorithm	ImageJ	https://imagej.nih.gov/ij/		
Software; Algorithm	Graph Pad Prism	https://www.graphpad.com/scientific-software/prism/		
Software; Algorithm	Statistica	https://www.tibco.com/		
Software; Algorithm	ANYMAZE	http://www.anymaze.co.uk/		
Software; Algorithm	ZEN	https://www.zeiss.com/microscopy/us/products/microscope-software/zen-lite.html		
Software; Algorithm	AxoScope 10.5	https://www.moleculardevices.com/		
Software; Algorithm	Proteome Discoverer	https://www.thermofisher.com/order/catalog/product/OPTON-30795		

Resource Type	Specific Reagent or Resource	Source or Reference	Identifiers	Additional Information
Software; Algorithm	Perseus	https://www.biochem.mpg.de/5111810/perseus		